

# High-spin spectroscopy in $^{207}\text{At}$ : Evidence of a $29/2^+$ isomeric state

Khamosh Yadav,<sup>1</sup> A. Y. Deo,<sup>1,\*</sup> Madhu,<sup>1</sup> Dhananjaya Sahoo,<sup>1</sup> P. C. Srivastava,<sup>1</sup>  
Saket Suman,<sup>2</sup> S. K. Tandel,<sup>2</sup> A. Sharma,<sup>3</sup> I. Ahmed,<sup>4</sup> K. Katre,<sup>4</sup> K. Rojeeta  
Devi,<sup>4</sup> Sunil Dutt,<sup>4</sup> Sushil Kumar,<sup>4</sup> Yashraj,<sup>4</sup> S. Muralithar,<sup>4</sup> and R. P. Singh<sup>4</sup>

<sup>1</sup>*Department of Physics, Indian Institute of Technology Roorkee, Roorkee 247667, India*

<sup>2</sup>*School of Physical Sciences, UM-DAE Centre for Excellence in Basic Sciences, University of Mumbai, Mumbai 400098, India*

<sup>3</sup>*Department of Physics, Himachal Pradesh University, Shimla 171005, India*

<sup>4</sup>*Inter-University Accelerator Centre, Aruna Asaf Ali Marg, New Delhi 110067, India*

(Dated: April 10, 2023)

Yrast and near-yrast states above the known  $25/2^+$  isomer in  $^{207}\text{At}$  are established for the first time. The level scheme is extended up to  $47/2\hbar$  and 6.5 MeV with the addition of about 60 new  $\gamma$ -ray transitions. The half-life of the  $25/2^+$  isomer is revisited and a value of  $T_{1/2} = 107.5(9)$  ns is deduced. Evidence of a hitherto unobserved  $29/2^+$  isomer in  $^{207}\text{At}$  is presented. A systematic study of  $B(E3)$  values for the transitions de-exciting the  $29/2^+$  isomer in the neighboring odd- $A$  At isotopes suggests a half-life in the 2–4  $\mu\text{s}$  range for this state in  $^{207}\text{At}$ . The experimental results are compared with large-scale shell-model calculations performed using the KHM3Y effective interaction in the  $Z = 50$ –126,  $N = 82$ –184 model space and an overall good agreement is noted between the theory and the experiment. A qualitative comparison of the excited states and the isomers with analogous states in neighboring nuclei provides further insight into the structure of  $^{207}\text{At}$ .

## I. INTRODUCTION

Neutron-deficient nuclei in the region around the doubly magic  $^{208}\text{Pb}$  nucleus reveal a large variety of structural properties and phenomena such as shape coexistence, shears bands, superdeformed bands, and various kinds of low- and high-spin isomers [1–4]. Nuclei in the vicinity of both the proton and neutron shell closures exhibit spherical or near-spherical shapes arising due to intrinsic degrees of freedom (*i.e.* particle-hole excitations) [5]. However, the onset of collective excitations is evident in nuclei with several valence particles or holes outside the shell closures. In this respect, Po and At isotopes offer a suitable ground for understanding the shape evolution. The level structures in the Po isotopes near the neutron shell closure ( $N = 126$ ) have been interpreted in terms of intrinsic degrees of freedom using the shell-model approach, while the collective modes of excitation have been observed in the lighter Po isotopes [6, 7]. The Po isotopes with  $N \approx 112$ , viz.  $^{192}$ – $^{195}\text{Po}$  [4], exhibit oblate-deformed structures, and subsequently evolve into prolate deformation as the  $N = 104$  neutron mid-shell is approached [8]. Experimentally, the shape evolution, as one moves from the spherical to the deformed regime, is manifested in the enhancement of the  $E2$  transition strengths and the energy systematics of the first excited  $2^+$  and  $4^+$  states [6, 7]. A recent study on the low-lying level structures in  $^{204}\text{Po}$  and  $^{206}\text{Po}$  [7] isotopes reports that the transition from single-particle to collective-excitation modes with decreasing neutron number occurs below  $^{206}\text{Po}$ . With one extra proton, the level structures in odd- $A$  At isotopes can be interpreted in terms of an unpaired proton coupled to the even-even

core of the corresponding Po isotone. Hence, the odd- $A$  At nuclei are expected to inherit structural properties and phenomena from the corresponding Po core, which is indeed reflected in the earlier studies [9–22].

Several high-spin isomers have been reported in nuclei with  $Z > 82$  and  $N \leq 126$ , which further motivates nuclear structure studies in the above near-spherical regime. The study of nuclear isomers is pivotal as it provides key inputs for understanding the structure of nuclei and to test the predictions of the shell model [23]. Among the neutron-deficient even- $A$  Po isotopes, isomeric  $8^+$ ,  $9^-$ , and  $11^-$  states have been observed in  $^{200}$ – $^{208}\text{Po}$  [24–32]. The hindrance in the decay of the  $8^+$  state has been understood in terms of small energy difference between the  $6^+$  and  $8^+$  states of the  $\pi(h_{9/2}^2)$  multiplet, while the metastable nature of the  $9^-$  and  $11^-$  states is attributed to a change in the single-particle configuration of the isomeric state and the one to which it decays [24–32]. Similarly, several high-spin isomers have also been reported in At isotopes. An isomeric  $13/2^+$  level, which originates from the  $\pi(i_{13/2})$  configuration, has been observed in  $^{197}$ – $^{203}\text{At}$  isotopes [11–13]. In  $^{197,199}\text{At}$  nuclei [10, 11], the isomeric  $13/2^+$  state is suggested to have oblate deformation and is populated by a strongly coupled rotational band, while it is known to have weak oblate deformation in  $^{201}\text{At}$  [12]. Also,  $25/2^+$  isomeric states with  $T_{1/2}$  in the range of  $\approx 14$ –108 ns were reported in  $^{203,205,207}\text{At}$  [13–16]. Furthermore, an isomeric  $29/2^+$  state has been observed in odd- $A$  At isotopes with  $199 \leq A \leq 211$  [12–15, 17–19], except in  $^{207}\text{At}$  [16]. The systematic presence of the  $29/2^+$  isomeric level in odd- $A$  At isotopes is one of the motivations for the detailed high-spin study along with a search for the  $29/2^+$  isomer in  $^{207}\text{At}$ . A comprehensive spectroscopic study in  $^{207}\text{At}$  ( $Z = 85$ ,  $N = 122$ ) is also needed for understanding the shape evolution along the isotopic chain in

\* Corresponding author: [ajay.deo@ph.iitr.ac.in](mailto:ajay.deo@ph.iitr.ac.in)



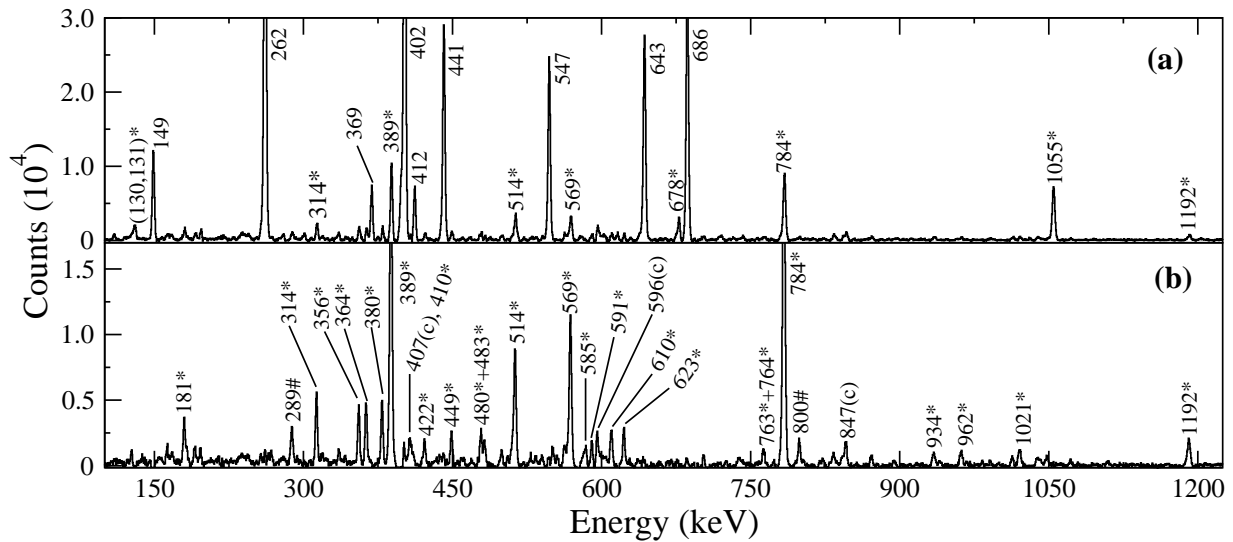


FIG. 2. The  $\gamma$ -ray spectra illustrating the transitions detected within (a)  $\pm 100$  ns prompt, and (b) 100–275 ns *early* coincidence windows of the 220-keV  $\gamma$  ray. The new  $\gamma$  rays from  $^{207}\text{At}$ , which are firmly placed in the level scheme, are marked with an asterisk. The  $\gamma$ -ray transitions marked with symbol “#” also belong to  $^{207}\text{At}$ . However, their position in the level scheme could not be ascertained. The transitions labeled with symbol (c) are contaminant lines.

Energy Photon Spectrometer (LEPS) at the time of the experiment. The detectors were located at five different angles,  $32^\circ$ ,  $57^\circ$ ,  $90^\circ$ ,  $123^\circ$ , and  $148^\circ$  with respect to the beam direction. The data were acquired using a VME-based data acquisition system [34] and written to a disk in the ROOT [35] tree format. The standard  $^{152}\text{Eu}$  and  $^{133}\text{Ba}$  sources were used to obtain the energy calibration and relative  $\gamma$ -ray efficiencies of the clover Ge detectors. The data collected at the three beam energies were combined to generate various two- and three-dimensional histograms, which aid in establishing the coincidence relationships, ordering of the levels, lifetimes of the isomeric states, and the multipolarity of the  $\gamma$ -ray transitions. The software packages ROOT [35] and RADWARE [36] were used to analyze these histograms.

The electronic time of each  $\gamma$  ray was obtained from the TDC signal from the corresponding clover detector. The coincidence windows used to construct the histograms were defined by the time difference between the corresponding  $\gamma$  rays. In order to construct symmetric two- and three-dimensional histograms, the  $\gamma$  rays detected within 100 ns of each other were utilized. The coincidences occurring within 100–200 ns of each other were subtracted from the above histograms to account for random events. The resulting prompt histograms were utilized to establish coincidence relationships among the observed  $\gamma$ -ray transitions. Furthermore, an asymmetric  $\gamma$ – $\gamma$  matrix, termed as an *early-delayed* matrix, was also constructed using the  $\gamma$  rays detected within 100–275 ns of each other. The *early* and *delayed* transitions for the above matrix are classified based on their relative electronic times. This matrix was utilized to investigate the isomers and the correlations between the transitions across the isomeric states. It may be noted that the use-

ful range of the TDC was 0–275 ns.

The multipolarity of the  $\gamma$ -ray transitions were assigned on the basis of the Directional angular Correlation from the Oriented states (DCO) ratio measurements [37] or intensity balance considerations. The experimental DCO ratio ( $R_{\text{DCO}}$ ) for a transition of interest was defined as the ratio of its intensities in the coincidence spectra from the detectors at  $148^\circ/32^\circ$  to that at  $90^\circ$  with respect to the beam direction. For the present detection setup, the  $R_{\text{DCO}}$  value was found to be close to 1.0 (0.5) for a stretched quadrupole (dipole) transition with a gate on a stretched quadrupole transition, and a value of  $R_{\text{DCO}} \approx 2.0$  (1.0) was observed for a stretched quadrupole (dipole) transition in a dipole gate. More details on the procedure of the DCO ratio measurements can be found elsewhere [38, 39]. The parity of the excited levels was assigned on the basis of the electric or magnetic nature of the feeding and/or depopulating  $\gamma$ -ray transitions. The electromagnetic nature of the  $\gamma$ -ray transitions, whenever possible, was confirmed from the polarization asymmetry ( $\Delta_{\text{asym}}$ ) measurements [40]. For this purpose, two asymmetric  $\gamma$ – $\gamma$  matrices were generated with one axis comprising the energies of the  $\gamma$  rays scattered in the perpendicular or parallel crystals of the  $90^\circ$  detectors with respect to the reaction plane and the other axis corresponding to the  $\gamma$ -ray energies detected in the remaining detectors. Furthermore, the  $\Delta_{\text{asym}}$  was defined as

$$\Delta_{\text{asym}} = \frac{a(E_\gamma)N_\perp - N_\parallel}{a(E_\gamma)N_\perp + N_\parallel}, \quad (1)$$

where  $N_\perp$  ( $N_\parallel$ ) are the counts recorded in the perpendicular (parallel) segments of the  $90^\circ$  detectors, where  $a(E_\gamma)$  is a geometrical asymmetry factor which is defined as the

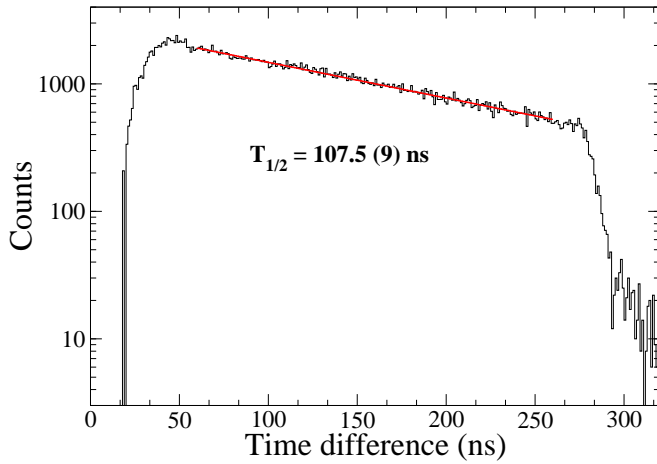


FIG. 3. Time-distribution curve (in black color) to determine half-life of the  $25/2^+$  state. The curve is obtained by subtracting the electronic timing of the 784-keV transition from that of the 220-keV transition. The contributions of the prompt time-distribution and background are removed from the curve. The solid line (in red color) corresponds to an exponential fit to the time-distribution curve.

ratio of  $N_{\parallel}$  and  $N_{\perp}$  for the  $\gamma$  rays from an unpolarized radioactive source. The experimental values of  $a(E_{\gamma})$  obtained using a  $^{152}\text{Eu}$  source were plotted as a function of  $\gamma$ -ray energies and fitted with a function,  $a(E_{\gamma}) = a_0 + a_1 E_{\gamma}$ . The coefficients  $a_0$  and  $a_1$  were found to be 1.029(3) and  $-7.96(363) \times 10^{-6}$ , respectively. The positive and negative values of the  $\Delta_{\text{asym}}$  signify electric and magnetic nature of the  $\gamma$ -ray transitions of interest, respectively.

### III. RESULTS

Excited states in  $^{207}\text{At}$  were studied earlier through  $^{204}\text{Pb}(^6\text{Li}, 3n)^{207}\text{At}$  heavy-ion fusion evaporation reaction [16]. This work had established a total of ten excited levels in  $^{207}\text{At}$  including a  $25/2^+$  isomer with  $T_{1/2} = 108(2)$  ns at 2117 keV [16]. An extended level scheme of  $^{207}\text{At}$  deduced from the present study is shown in Fig. 1. The level scheme below the  $25/2^+$  isomer [16] is revisited and found to be consistent with the present data. Figure 2(a) illustrates the  $\gamma$ -ray transitions in coincidence with the 220-keV  $\gamma$  ray which de-excites the  $25/2^+$  isomer. In addition to the known transitions, several new transitions were observed in the above coincidence spectrum. Figure 2(b) presents  $\gamma$ -ray transitions which precede the 220-keV  $\gamma$  ray within a 100–275 ns time window. The relative enhancement in the intensity of the 314-, 389-, 514-, 569-, 784-, and 1192-keV  $\gamma$  rays in Fig. 2(b) compared to those in Fig. 2(a) confirms the isomeric nature of the  $25/2^+$  state. In addition to the above transitions, many new transitions were also observed in the *delayed* gate of the 220-keV  $\gamma$  ray as evident from the Fig. 2(b).

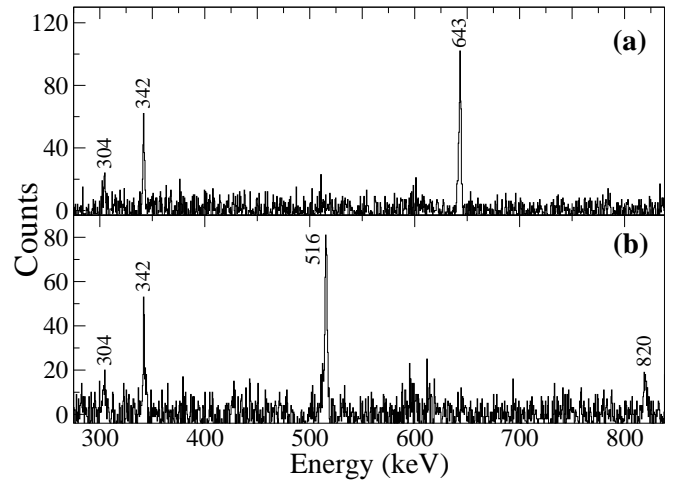


FIG. 4. The coincidence spectra with double gates on the (a) 472-, 516-keV, and (b) 472-, 643-keV transitions to illustrate evidence of the new 304-, 342-, and 820-keV  $\gamma$  rays.

It was further observed that these new transitions were also present in all the *early* coincidence spectra obtained with gates on the previously known transitions following the decay of the  $25/2^+$  isomer, which unambiguously confirms their assignment to  $^{207}\text{At}$ . The coincidence relationships of the new transitions feeding the 2117-keV isomeric level and their placement in the level scheme are discussed in Sec. III(A) in detail.

The half-life of the known  $25/2^+$  isomer at 2117 keV was also revisited using the decay-curve analysis method as shown in Fig. 3. This method is suitable to determine lifetimes significantly greater than the full width at half-maximum (FWHM) of a prompt time distribution [41]. For the present detector system, the FWHM was found to be around 50 ns for the feeding and decaying  $\gamma$ -ray energies of around 500 keV. The deduced half-life,  $T_{1/2} = 107.5(9)$  ns, was found to be in good agreement with the value reported earlier [16].

Several new transitions were also identified below the  $25/2^+$  isomer. For example, a 1055-keV transition was found to be in coincidence with the 220-keV  $\gamma$  ray as shown in Fig. 2(a). It was also observed to be in coincidence with all the earlier known transitions above the 1085-keV level. Sjoreen *et al.* [16] had established a  $13/2^-$  level at 1055 keV. Also, the presence of an unobserved  $\gamma$  ray of 30 keV between the  $15/2^-$  and  $13/2^-$  levels at 1085- and 1055-keV, respectively, was inferred on the basis of  $\gamma - \gamma$  coincidence relationships. The present study also supports these observations and suggests a new direct decay path to the ground state via the 1055-keV  $\gamma$  ray.

Furthermore, a sequence of 472-, 516-, and 342-keV  $\gamma$ -ray transitions was established above the  $11/2^-$  level at 643 keV. It may be noticed that Sjoreen *et al.* [16] had suggested a tentative 340-keV  $\gamma$  ray as opposed to the 342 keV one seen in this work. The  $\gamma$ -ray spectra presented



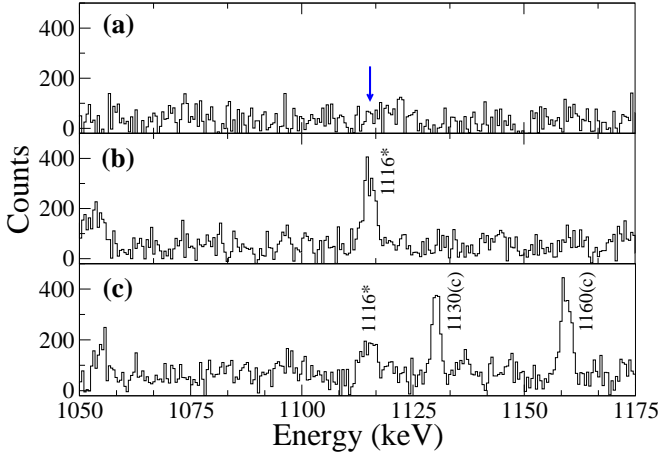


FIG. 5. The  $\gamma$ -ray coincidence spectra in a gate on the (a) 472-, (b) 516-, and (c) 342-keV  $\gamma$ -ray transitions illustrating the absence/presence of the 1116-keV  $\gamma$  ray in coincidence with the gating transitions. The transitions labeled with (c) in the last panel are contaminants from  $^{63}\text{Cu}$  and  $^{67}\text{Ga}$  produced through reactions of the beam with the Fe target frame.

in Fig. 4 clearly establish the coincidence relationships of the new 342-keV transition with the known 643-, 472-, and 516 keV  $\gamma$  rays. These spectra also confirm the placement of the new 304- and 820-keV  $\gamma$ -ray transitions as shown in Fig. 1. Also, a new 1116-keV  $\gamma$ -ray was found in coincidence with the 516- and 342-keV  $\gamma$  rays, but not with the 472-keV transition as illustrated in Fig. 5. The 1116-keV  $\gamma$  ray de-excites the associated level directly to the ground state. The spin assignment of  $I = (13/2)$  and  $(15/2)$  to the 1116-, and 1631-keV levels, respectively, is adopted from Ref. [16]. A spin assignment of  $I = (17/2)$  to the 1973-keV level as well as positive parity for the states under consideration are proposed on the basis of similarities in their decay paths with those in the lighter odd- $A$  At isotopes, and will be discussed in detail in Sec. IV(A).

The remaining level scheme below the  $25/2^+$  isomer was investigated using similar  $\gamma-\gamma$  coincidence relationships, relative intensity considerations and the energy-sum technique. The procedure of the relative intensity measurements is discussed later in this section. The energy of the  $\gamma$ -ray transitions below the  $25/2^+$  isomer and their relative  $\gamma$ -ray intensities are listed in Table I. The spin-parity assignments of the levels below the  $25/2^+$  isomer, except for the 1115.5-, 1631.0-, and 1973.2-keV levels, are adopted from Ref. [16].

#### A. Level structure above the $25/2^+$ isomer

As mentioned earlier, excited states in  $^{207}\text{At}$  were studied previously by Sjöreen *et al.* up to  $25/2^+$  isomer [16]. However, no excited states were known above this isomeric level. The present study extends the level scheme

TABLE I. Table of  $\gamma$ -ray energies ( $E_\gamma$ ), corresponding level energies ( $E_i$ ), relative  $\gamma$ -ray intensity ( $I_\gamma$ ), and spin-parity of the initial ( $I_i^\pi$ ) and final ( $I_f^\pi$ ) levels below the  $25/2^+$  isomer in  $^{207}\text{At}$ . The relative intensities are quoted in percent by normalizing their values with respect to the intensity of the 643-keV transition, which is assumed to be 100. The listed spin-parities are adopted from Ref. [16], except for the 1115.5-, 1631.0-, and 1973.2-keV levels. See the text for their spin-parity assignments. The uncertainties in the  $\gamma$ -ray energies and relative intensities have contributions from both statistical and systematic factors. The systematic uncertainty in  $I_\gamma$  is considered to be 5% of the relative  $\gamma$ -ray intensity.

$E_\gamma$ (keV)	$E_i$ (keV)	$I_\gamma$	$I_i^\pi$	$I_f^\pi$
(30) <sup>a</sup>	1084.6(2)	—	$15/2^-$	$13/2^-$
(43) <sup>a</sup>	686.3(1)	—	$13/2^-$	$11/2^-$
130.5(3)	1495.1(2)	4.3(2) <sup>b</sup>	$21/2^-$	—
131.0(5)	1364.6(5)	—	—	$17/2^-$
149.0(1)	1233.6(1)	21.3(12)	$17/2^-$	$15/2^-$
219.6(1)	2116.6(1)	53.8(31)	$25/2^+$	$23/2^-$
261.5(1)	1495.1(2)	134.7(77)	$21/2^-$	$17/2^-$
304.0(4)	1935.3(5)	<1	—	$(15/2^+)$
342.2(3)	1973.2(3)	2.8(2)	$(17/2^+)$	$(15/2^+)$
368.7(2)	1054.8(4)	14.3(8)	$13/2^-$	$13/2^-$
398.2(2)	1084.6(2)	16.9(10)	$15/2^-$	$13/2^-$
401.9(1)	1897.0(1)	113.4(65)	$23/2^-$	$21/2^-$
412.0(2)	1054.8(4)	13.0(7)	$13/2^-$	$11/2^-$
441.4(1)	1084.6(2)	60.5(34)	$15/2^-$	$11/2^-$
472.3(2)	1115.5(4)	6.7(4)	$(13/2^+)$	$11/2^-$
515.5(3)	1631.0(3)	3.7(2)	$(15/2^+)$	$(13/2^+)$
547.3(1)	1233.6(1)	56.1(32)	$17/2^-$	$13/2^-$
643.2(1)	643.2(1)	100.0(52)	$11/2^-$	$9/2^-$
678.3(2)	1364.6(5)	9.7(6)	—	$13/2^-$
686.3(1)	686.3(1)	109.6(57)	$13/2^-$	$9/2^-$
722.4(3)	1956.0(4)	1.7(1)	—	$17/2^-$
819.8(3)	1935.3(5)	1.2(1)	—	$(13/2^+)$
871.4(2)	1956.0(4)	5.2(3)	—	$15/2^-$
1054.8(1)	1054.8(4)	36.2(19)	$13/2^-$	$9/2^-$
1115.5(4)	1115.5(4)	<1	$(13/2^+)$	$9/2^-$

<sup>a</sup> Unobserved  $\gamma$  ray, but its presence is inferred from the coincidence relationships.

<sup>b</sup> Summed relative  $\gamma$ -ray intensity of the 130.5- and 131-keV  $\gamma$  rays.

beyond the  $25/2^+$  isomer up to  $47/2\hbar$  and  $E_x \approx 6.5$  MeV. As illustrated in Fig. 2(b), many new transitions were identified which precede the 220-keV  $\gamma$  ray. Four new sequences consisting of about 30 new  $\gamma$ -ray transitions were established, which feed the known  $25/2^+$  isomeric state.

The *early*  $\gamma$ -ray spectra obtained with gates on the  $\gamma$  rays following the decay of the  $25/2^+$  isomer indicate that the 784- and 389-keV transitions are the strongest transitions above the isomer. These transitions were also found to be in mutual coincidence [see Fig. 6(a)], which justifies their placement above the 2117-keV isomeric level as shown in Fig. 1. A cascade of new transitions viz. 514-, 356-, and 591 keV, was found to be in coincidence with the above transitions. These transitions were placed

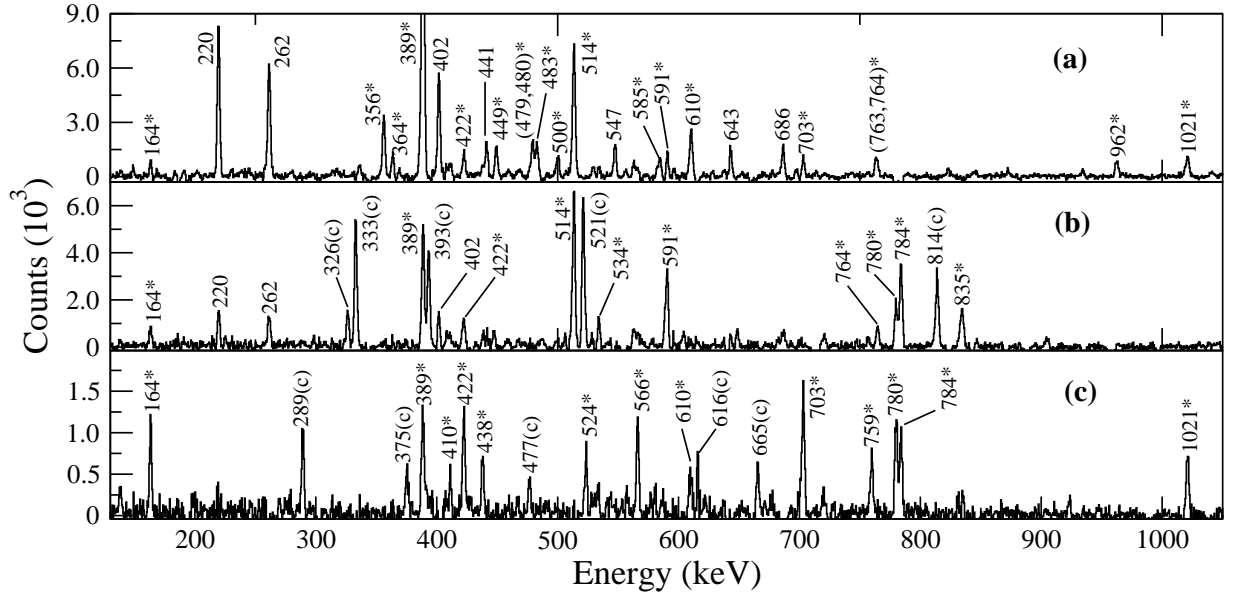


FIG. 6. The  $\gamma$ -ray spectra illustrating the transitions in coincidence with the (a) 784-, (b) 356-, and (c) 500-keV  $\gamma$  rays. The transitions marked with an asterisk are the new  $\gamma$  rays assigned to  $^{207}\text{At}$ , while those marked with a symbol (c) are contaminants mainly from  $^{196}\text{Pt}$ ,  $^{206,207}\text{Po}$ , and  $^{206}\text{At}$ .

above the 3289-keV level in sequence “A” in the descending order of their relative intensities as shown in Fig. 1. Another cascade of 1021-, 703-, 500-, 422-, 438-, and 164-keV transitions, labeled as sequence “D” in Fig. 1, was also identified to be in coincidence with the 784- and 389-keV  $\gamma$  rays. The prompt coincidence spectra illustrated in Fig. 6 support the coincidence relationships of these transitions. Furthermore, the new 483-, 479-, 449-, 962-, and 364-keV transitions were also observed in coincidence with the 389- and 784-keV  $\gamma$  rays. These transitions were placed in sequence “B” as shown in Fig. 1 by using their relative intensities and coincidence relationships.

The coincidence relationships and placements of the new 780-, 759-, 566-, and 524-keV transitions observed in Fig. 6(c) are discussed in the next section.

Several other new transitions, viz., the 569-, 1192-, 623-, 181-, 380-, and 314 keV, were also observed in *early* coincidence with the 220-keV [see Fig. 2(b)] as well as with the other transitions following the decay of the  $25/2^+$  isomer. These transitions were not observed in coincidence with the transitions in sequences “A”, “B”, and “D”, except the 364-keV one (see Fig. 6). Two illustrative prompt spectra with gates on the 1192- and 623-keV transitions are presented in Fig. 7. The observed new transitions were placed in sequence “C”, which directly feeds the  $25/2^+$  isomer.

Furthermore, some transitions were identified in the present work which bypass the  $25/2^+$  isomer. Two transitions, viz. the 780- and 1230-keV ones were observed in mutual coincidence and placed above the  $21/2^-$  level at 1495 keV on the basis of their relative intensities and coincidence relationships. In addition, the presence of new 197- and 364-keV transitions and their placement in the

level scheme connect the sequence “C” with the one of the bypassing transitions. Also, it was noticed that the 364-keV  $\gamma$  ray is a doublet and both the components are in coincidence with each other. The above coincidence relationship and coincidence of the 364-keV  $\gamma$  ray with all the transitions in sequence “C” suggest the presence of an unobserved 69-keV transition between the 4252- and 4183-keV levels. However, a possibility of the presence of an another 364-keV transition which may directly feed the 4183-keV level can not be discarded.

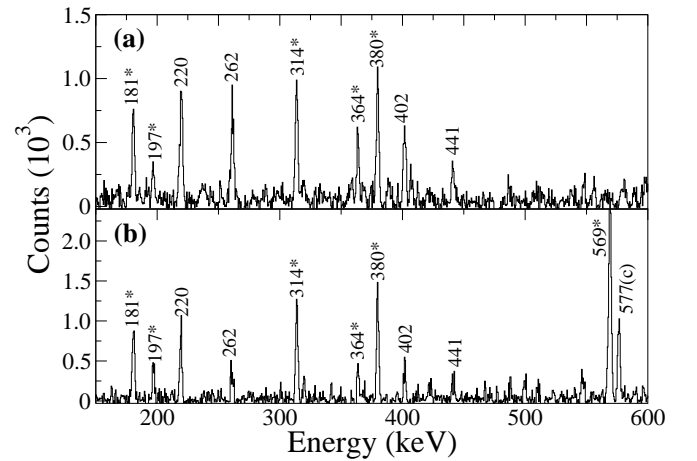


FIG. 7. The  $\gamma$  ray coincidence spectra obtained with gate on the (a) 1192- and (b) 623-keV  $\gamma$ -ray transitions. The transitions marked with an asterisk are the new transitions from  $^{207}\text{At}$ . The 577-keV transition marked with symbol (c) is contamination from  $^{207}\text{Po}$ .

TABLE II. Table of  $\gamma$ -ray energies ( $E_\gamma$ ), corresponding initial level energies ( $E_i$ ), spin-parity of the initial ( $I_i^\pi$ ) and final ( $I_f^\pi$ ) levels, relative  $\gamma$ -ray intensity ( $I_\gamma$ ),  $R_{\text{DCO}}$ ,  $\Delta_{\text{asym}}$  values and assigned multipolarity of the  $\gamma$ -ray transitions de-exciting the levels above the  $25/2^+$  isomer. The relative intensities are quoted in percent by normalizing their values with respect to the intensity of the 643-keV transition, which is assumed to be 100. The uncertainties in the  $\gamma$ -ray energies, relative intensities and  $R_{\text{DCO}}$  values have contributions from both statistical and systematic factors. The systematic uncertainty in  $I_\gamma$  is considered to be 5% of the relative  $\gamma$ -ray intensity.

$E_\gamma$ (keV)	$E_i$ (keV)	$I_i^\pi$	$I_f^\pi$	$I_\gamma$	$R_{\text{DCO}}$	$\Delta_{\text{asym}}$	Multipolarity
(69) <sup>a</sup>	4251.8(4)	35/2 <sup>-</sup>	33/2 <sup>(+)</sup>	—			
(70) <sup>a</sup>	3289.3(2)	33/2 <sup>+</sup>	31/2 <sup>+</sup>	—			
124.7(3)	3289.3(2)	33/2 <sup>+</sup>	33/2 <sup>+</sup>	1.4(1)			
163.6(2)	6538.4(3)	47/2	45/2	3.7(2)	0.52(4) <sup>b</sup>		$D$
180.6(2)	3489.4(3)	29/2 <sup>(+)</sup>	27/2 <sup>-</sup>	4.5(3)	1.24(9) <sup>c</sup>		$D$
193.1(3)	2149.1(4)	—	—	3.8(2)			
196.8(3)	3505.3(5)	29/2 <sup>(-)</sup>	27/2 <sup>-</sup>	3.7(2)			
252.0(3)	2149.1(4)	—	23/2 <sup>-</sup>	1.1(1)			
259.1(4)	4159.2(5)	37/2 <sup>+</sup>	35/2 <sup>+</sup>	<1			
264.7(2)	3952.8(3)	37/2	35/2 <sup>+</sup>	3.8(2)	0.46(3) <sup>b</sup>		$D$
313.7(2)	4182.9(3)	33/2 <sup>(+)</sup>	31/2 <sup>(+)</sup>	9.7(5)	1.01(7) <sup>c</sup>	-0.112(29)	$M1$
356.4(2)	4159.2(5)	37/2 <sup>+</sup>	35/2 <sup>+</sup>	9.8(6)	0.48(3) <sup>b</sup>	-0.087(21)	$M1$
363.6(2)	4615.4(3)	37/2 <sup>(-)</sup>	35/2 <sup>-</sup>	5.4(3)	0.50(4) <sup>b</sup>	-0.025(35)	$(M1 + E2)$
363.8(5)	3869.2(5)	31/2 <sup>(+)</sup>	29/2 <sup>(-)</sup>	7.5(6)			
379.8(2)	3869.2(5)	31/2 <sup>(+)</sup>	29/2 <sup>(+)</sup>	5.2(3)	0.94(7) <sup>c</sup>	-0.139(33)	$M1$
388.6(1)	3289.3(2)	33/2 <sup>+</sup>	29/2 <sup>+</sup>	36.3(20)	1.07(8) <sup>b</sup>	0.101(18)	$E2$
410.5(4)	4310.3(4)	37/2 <sup>+</sup>	35/2 <sup>+</sup>	<1			
422.5(2)	5936.6(3)	43/2 <sup>(+)</sup>	41/2 <sup>+</sup>	6.3(4)	0.54(4) <sup>b</sup>	-0.016(15)	$(M1 + E2)$
438.2(3)	6374.8(3)	45/2	43/2 <sup>(+)</sup>	3.4(2)	0.60(5) <sup>b</sup>		$D$
449.4(2)	4251.8(4)	35/2 <sup>-</sup>	35/2 <sup>+</sup>	5.6(3)	1.17(9) <sup>b</sup>	-0.077(26)	$E1, \Delta I = 0$
479.3(3)	4251.8(4)	35/2 <sup>-</sup>	33/2	1.5(1)	1.21(9) <sup>c</sup>		$D$
479.6(3)	3380.3(4)	—	29/2 <sup>+</sup>	2.4(2)			
483.2(2)	3772.5(2)	33/2	33/2 <sup>+</sup>	3.5(2)	0.86(6) <sup>b</sup>		$D, \Delta I = 0$
487.6(1)	2384.6(1)	29/2 <sup>+</sup>	23/2 <sup>-</sup>	66.5(38)			
500.4(2)	5514.1(5)	41/2 <sup>+</sup>	39/2 <sup>+</sup>	6.1(4)	0.44(3) <sup>b</sup>	-0.045(21)	$M1$
513.5(1)	3802.8(2)	35/2 <sup>+</sup>	33/2 <sup>+</sup>	22.1(13)	0.48(3) <sup>b</sup>	-0.066(18)	$M1$
523.5(2)	3688.1(3)	35/2 <sup>+</sup>	33/2 <sup>+</sup>	14.3(8)	1.02(8) <sup>c</sup>	-0.044(21)	$M1$
534.4(3)	4693.6(3)	39/2	37/2 <sup>+</sup>	2.0(1)	1.03(8) <sup>c</sup>		$D$
566.3(2)	4254.4(3)	37/2 <sup>+</sup>	35/2 <sup>+</sup>	6.8(4)	1.10(8) <sup>c</sup>	-0.054(21)	$M1$
569.3(1)	2685.9(2)	27/2 <sup>+</sup>	25/2 <sup>+</sup>	15.1(8)	0.86(6) <sup>c</sup>	-0.091(32)	$M1$
584.8(3)	3485.5(4)	—	29/2 <sup>+</sup>	1.7(1)			
590.6(2)	4749.8(3)	39/2	37/2 <sup>+</sup>	4.8(3)	0.92(7) <sup>c</sup>		$D$
610.5(2)	3899.8(3)	35/2 <sup>+</sup>	33/2 <sup>+</sup>	8.5(5)	0.44(3) <sup>b</sup>	-0.072(23)	$M1$
622.9(2)	3308.8(4)	27/2 <sup>-</sup>	27/2 <sup>+</sup>	4.1(2)	2.22(16) <sup>c</sup>		$D, \Delta I = 0$
654.0(3)	2149.1(4)	—	21/2 <sup>-</sup>	2.4(1)			
703.4(2)	5013.7(4)	39/2 <sup>+</sup>	37/2 <sup>+</sup>	3.7(2)	0.50(4) <sup>b</sup>	-0.040(28)	$M1$
759.4(3)	5013.7(4)	39/2 <sup>+</sup>	37/2 <sup>+</sup>	2.3(1)	0.95(7) <sup>c</sup>	-0.027(51)	$(M1 + E2)$
763.2(3)	3663.9(4)	—	29/2 <sup>+</sup>	2.5(2)			
764.4(3)	5514.1(5)	41/2 <sup>+</sup>	39/2	1.9(1)	0.98(7) <sup>c</sup>		$D$
779.8(2)	2274.9(3)	25/2 <sup>-</sup>	21/2 <sup>-</sup>	9.6(5)	1.97(15) <sup>c</sup>	0.069(23)	$E2$
780.0(1)	3164.6(1)	33/2 <sup>+</sup>	29/2 <sup>+</sup>	42.0(24)	2.14(16) <sup>c</sup>	0.076(25)	$E2$
784.1(1)	2900.7(1)	29/2 <sup>+</sup>	25/2 <sup>+</sup>	54.4(30)	0.94(7) <sup>b</sup>	0.098(11)	$E2$
834.6(1)	3219.2(1)	31/2 <sup>+</sup>	29/2 <sup>+</sup>	31.0(18)	0.81(6) <sup>c</sup>	-0.029(25)	$M1$
854.0(2)	2349.1(3)	—	21/2 <sup>-</sup>	3.5(2)			
934.5(3)	4223.8(4)	35/2	33/2 <sup>+</sup>	2.6(2)	0.44(3) <sup>b</sup>		$D$
947.6(3)	4900.4(4)	—	37/2	1.9(1)			
962.5(2)	4251.8(4)	35/2 <sup>-</sup>	33/2 <sup>+</sup>	4.3(3)	0.53(4) <sup>b</sup>	0.188(33)	$E1$
1021.0(2)	4310.3(4)	37/2 <sup>+</sup>	33/2 <sup>+</sup>	5.7(3)	1.09(8) <sup>b</sup>	0.047(38)	$E2$
1071.9(3)	4361.2(4)	—	33/2 <sup>+</sup>	1.9(1)			
1191.9(2)	3308.8(4)	27/2 <sup>-</sup>	25/2 <sup>+</sup>	6.4(4)	1.11(8) <sup>c</sup>	0.155(56)	$E1$
1230.4(3)	3505.3(5)	29/2 <sup>(-)</sup>	25/2 <sup>-</sup>	2.1(1)	1.11(8) <sup>b</sup>		$Q$
1354.7(3)	5514.1(5)	41/2 <sup>+</sup>	37/2 <sup>+</sup>	2.8(2)			

<sup>a</sup> Unobserved  $\gamma$  ray, but its presence is inferred from the coincidence relationships.

<sup>b</sup>  $R_{\text{DCO}}$  value is obtained with a gate on a stretched quadrupole transition.

<sup>c</sup>  $R_{\text{DCO}}$  value is obtained with a gate on a pure dipole transition.

The spin-parity of the new levels above the  $25/2^+$  isomer were assigned on the basis of measured  $R_{\text{DCO}}$  and  $\Delta_{\text{asym}}$  values for the corresponding feeding and/or depopulating  $\gamma$ -ray transitions. As mentioned in Sec. II, the  $R_{\text{DCO}}$  value was found to be  $\approx 1.0$  when the gating transition and the  $\gamma$  ray of interest have the same multipolarity, while  $R_{\text{DCO}}$  was obtained to be  $\approx 2.0$  (0.5) for a stretched quadrupole (dipole) transition with a gate on a pure dipole (stretched quadrupole) one. These values were estimated from a few  $\gamma$  rays of known multipolarity from other nuclei populated in the same reaction. In  $^{207}\text{At}$ , the states above the  $25/2^+$  isomer are established for the first time in the present study. However, the isomeric nature of the  $25/2^+$  state [ $T_{1/2} = 107.5(9)$  ns] prevents the use of the transitions below the  $25/2^+$  isomer to obtain the  $R_{\text{DCO}}$  values for the new transitions feeding the isomer. Therefore, the  $R_{\text{DCO}}$  values for a few new transitions of the sequence “A” viz. 784-, 389-, 514-, and 356 keV, were determined using mutual gates and their multiplicities were assigned on the basis of consistency in their  $R_{\text{DCO}}$  values as discussed below. The  $R_{\text{DCO}}$  values for the 389-, 514-, and 356-keV transitions with a gate on the 784-keV  $\gamma$  ray are 1.07(8), 0.48(3), and 0.48(3), respectively. These values suggest that both the 784- and 389-keV  $\gamma$ -ray transitions are of the same multipolarity. Also, these  $R_{\text{DCO}}$  values collectively suggest that the 784- and 389-keV transitions are  $\Delta I = 2$  transitions, while the 514- and 356-keV transitions are of  $\Delta I = 1$  multipolarity. Furthermore, the  $R_{\text{DCO}}$  values for the 784-, 389-, and 514-keV transitions were determined using a gate on the 356-keV  $\gamma$  ray and found to be 2.00(14), 2.14(15), and 0.94(7), respectively. These values further corroborate the preceding multipolarity assignments of the 784-, 389-, 514- and 356-keV transitions. The  $R_{\text{DCO}}$  values for the remaining transitions in sequences “A–D” were obtained using the deduced multiplicities of the 784-, 389-, 514- and 356-keV transitions. Further, electric or magnetic nature of the new transitions were determined from the measured  $\Delta_{\text{asym}}$  values. The information on the  $\gamma$ -ray energies, relative intensities,  $R_{\text{DCO}}$  and  $\Delta_{\text{asym}}$  values for the transitions above the isomeric  $25/2^+$  level are listed in Table II.

### B. Evidence of a $29/2^+$ isomer at $E_x = 2385$ keV

An isomeric  $29/2^+$  state is known in  $^{199,201,203,205,209,211}\text{At}$  nuclei [12–15, 17, 18, 21]. However, such a state was not known in  $^{207}\text{At}$  [16]. In this section, we discuss the first evidence of the  $29/2^+$  isomeric state in  $^{207}\text{At}$ . Figure 8 illustrates the double-gated coincidence spectra of the (a) 402-, 262 keV, and (b) 402-, 220-keV transitions. It was observed that a strong 488-keV transition is present in Fig. 8(a), but not in Fig. 8(b). This indicates that the new 488-keV  $\gamma$  ray is in coincidence with the 262- and 402-keV transitions but not with the 220 keV, which in turn suggests that the 488-keV transition should be placed above the 402-keV

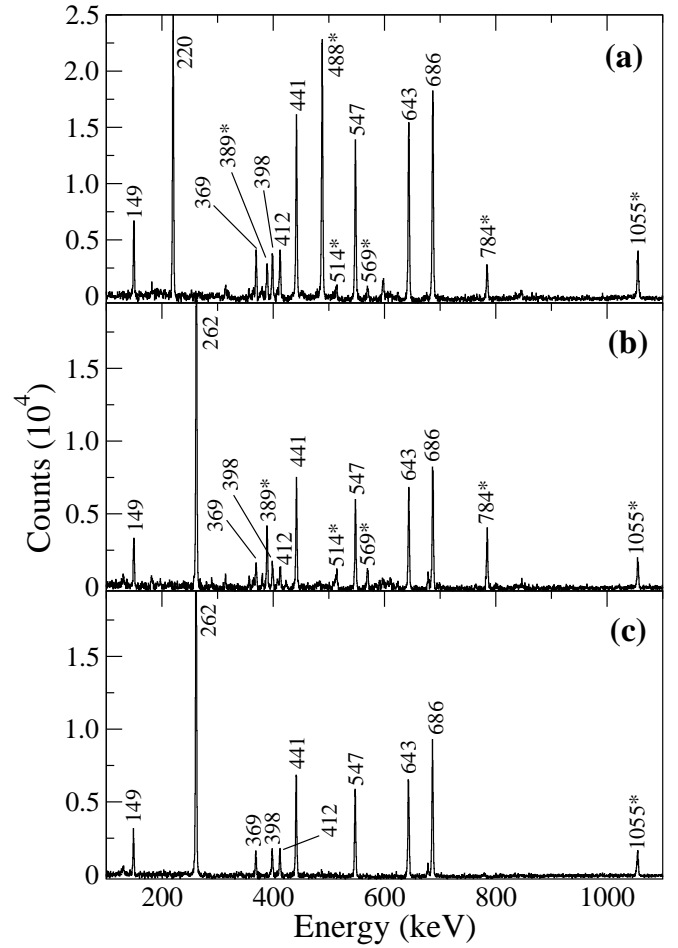


FIG. 8. Double-gated coincidence spectra illustrating  $\gamma$ -ray transitions in gates on the (a) 402-, 262-keV, (b) 402-, 220-keV, and (c) 402-, 488-keV  $\gamma$  rays within the prompt coincidence window. The new transitions are marked with asterisks.

$\gamma$  ray. The placement of the 488-keV  $\gamma$  ray introduces a new level at 2385 keV. Further, Fig. 8(c) depicts the  $\gamma$ -ray transitions in a double gate of the 402- and 488-keV  $\gamma$  rays. It may be noted that only transitions below the 1495-keV level (see Fig. 1) are observed in Fig. 8(c), which further corroborates the above placement of the new 488-keV  $\gamma$  ray. The absence of any prompt  $\gamma$  ray/s feeding the 2385-keV level indicates the presence of a long-lived isomeric state. Here, two possibilities may be considered. One could be that the 2385-keV level itself has a large half-life and therefore, the transition/s feeding the 2385-keV level could not be observed in the prompt coincidence (100 ns) with the 488-keV transition. Another possibility could be the presence of a closely-spaced higher-lying metastable state, which may de-excite to the 2385-keV level via one or more unobserved low energy and/or high multipole transitions. However, the second possibility can be discarded on the basis of the coincidence relationships of the transitions which are observed in *early* coincidence



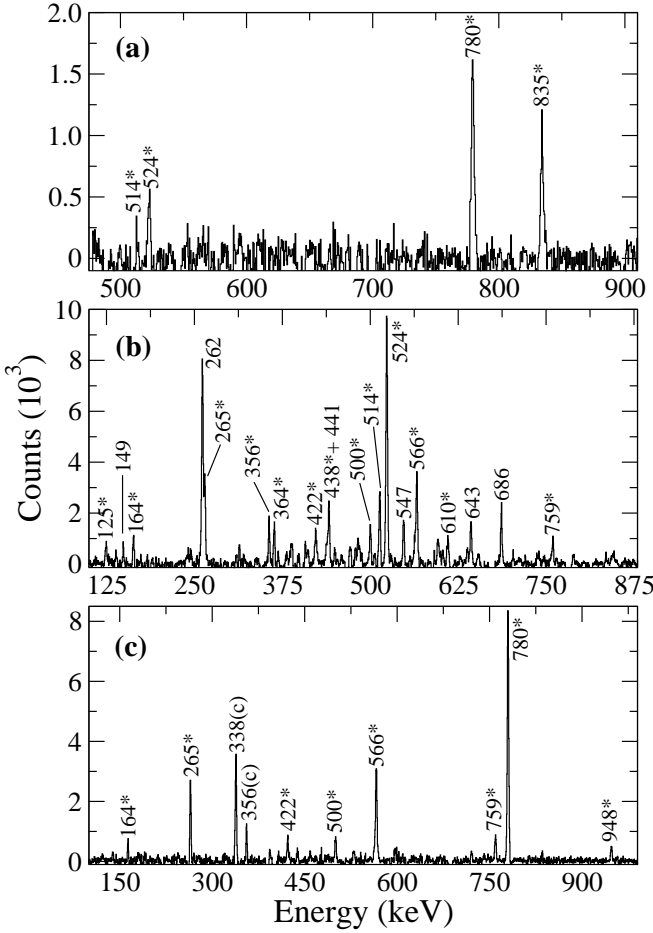


FIG. 9. Coincidence spectra illustrating  $\gamma$ -ray transitions in coincidence with the (a) 488-keV  $\gamma$  ray within a 100–275 ns *early* time window, (b) 780-, and (c) 524-keV  $\gamma$  rays within the prompt coincidence window. The new transitions from  $^{207}\text{At}$  are marked with asterisks. The transitions marked with the symbol (c) are contaminants from  $^{206}\text{Bi}$  and  $^{196}\text{Pt}$ .

with the new 488-keV  $\gamma$  ray as discussed below.

Figure 9(a) illustrates the transitions which precede the 488-keV  $\gamma$  ray within the 100–275 ns coincidence window. It was further observed that the strongest 780- and 835-keV  $\gamma$ -ray transitions are not in mutual coincidence, while the 780-keV one is in coincidence with a weaker 524-keV transition as evident from the two lower panels of Fig. 9. The new 780-, 524-, 265-, and 566-keV transitions were placed above the 2385-keV level as shown in Fig. 1 on the basis of their relative intensities and  $\gamma$ – $\gamma$  coincidence relationships. In addition, a new 759-keV transition was also observed in coincidence with the 780-, 524-, and 566-keV  $\gamma$  rays. The placement of the 759-keV  $\gamma$  ray connects the sequences “D” and “E” and also corroborates the placement of the new 780-keV transition.

Furthermore, the  $\gamma$ -ray transitions feeding the  $33/2^+$  level at 3289 keV in sequence “A” are also found in co-

incidence with the 780- and 835-keV transitions, but not with the 524-keV one [see Figs. 9(b), 9(c), and 6(b)]. It may be noted that the presence of the 262-, 441-, 547-, 643-, and 686-keV  $\gamma$ -ray transitions in Fig. 9(b) is attributed to their coincidence with another 780-keV transition which is placed above the 1495-keV level, as already mentioned in Sec. A. Also, a new 125-keV  $\gamma$  ray is found to be in coincidence with the 780-keV transition and with those feeding the  $33/2^+$  level at 3289 keV. The placement of the new 125-keV  $\gamma$  ray connects the sequences “A” and “E”, and hence further validates the positions of the new levels and transitions above the 2385-keV state as shown in Fig. 1. Moreover, the coincidences of the 835-keV line with the transitions feeding the 3289-keV level indicate the presence of an unobserved 70-keV transition. The placement of the transitions above the isomers in the sequences “A”, “D”, and “E” along with that of the 488-keV transition uniquely establishes a state at 2385 keV and the fact that it has a long half-life.

The spin-parity of the 2385-keV level is inferred based on the following considerations. The  $I^\pi = 39/2^+$  for the 5014-keV level is firmly established on the basis of the  $R_{\text{DCO}}$  and  $\Delta_{\text{asym}}$  values of the 703-, 1021-, 389- and 784-keV transitions. Now, this state is connected to the 2385-keV level via three  $\Delta I = 1$  transitions, viz., 759-, 566-, and 523-keV and one  $\Delta I = 2$  (780 keV) transition (see Table II). These measurements suggest  $I = 29/2$  for the 2385-keV level, which in turn leads to a possible  $E3$  or  $M3$  multipolarity for the 488-keV transition. Furthermore, intensity balance at the 1897-keV level (assuming  $I = 29/2$  for the 2385-keV level, as discussed above) supports  $E3$  multipolarity for the 488-keV transition, and hence  $I^\pi = 29/2^+$  is proposed for the 2385-keV state. Furthermore, the  $\Delta_{\text{asym}}$  values for the 780-, 523-, and 566-keV transitions suggest positive parity of the 3165-, 3688-, and 4254-keV levels in sequence “E”. The proposed spin-parity,  $I^\pi = 29/2^+$ , for the isomeric 2385-keV level is also supported by the energy systematics of the known  $29/2^+$  isomeric states in the neighboring odd- $A$  At isotopes and will be discussed in Sec. IV(B) in detail.

An attempt to determine the half-life of the isomeric state under consideration using the electronic timing method resulted in an almost flat time-difference distribution curve of the depopulating and feeding transitions. This suggests a significantly longer half-life as compared to the available narrow time range viz., 0–275 ns. However, a rough estimate of the half-life can be obtained as follows. The delayed gates of the 220- and 488-keV transitions were used to determine the intensities of the 784- and 780-keV transitions within the 100–275 ns *early* coincidence window, respectively. The ratio of the intensities of the 784- to 780-keV transitions was found to be 13.8. Now, the amount of the initial intensities (See Table. II) of the 784- and 780-keV transitions which decay within the 100–275 ns were determined with the help of radioactive decay law using the known half-life (107.9 ns) of the  $25/2^+$  state and assuming various values of  $T_{1/2}$  for the  $29/2^+$  state. The ratio of these intensities is to be

compared with the experimental value mentioned above. It was observed that, among the various values assumed for the half-life of the  $29/2^+$  state, a value of  $3.5 \mu\text{s}$  is able to reproduce the experimental ratio. In addition, a possible range of the half-life ( $2-4 \mu\text{s}$ ) is surmised on the basis of a systematic study of the  $B(E3)$  rates for the  $29/2^+ \rightarrow 23/2^-$  transitions in the neighboring odd-A At isotopes and will be discussed in IV(B).

### C. Intensity measurements

The relative intensities of the  $\gamma$ -ray transitions listed in Tables I and II were determined using the data at 87 MeV. In order to obtain the relative intensities of the transitions below the isomers, the pure 643- and 441-keV transitions were fitted in a spectrum obtained from the single-fold data. Further, the deduced intensities were normalized with respect to the intensity of the 643-keV  $\gamma$  ray, for which the intensity of 100 units was assumed. The relative  $\gamma$ -ray intensities of the 686-, 1055-, and 1116-keV transitions were determined by measuring the branching ratios of all the transitions feeding directly to the ground state in the efficiency corrected summed spectrum with the gates on the relevant transitions. Further, the efficiency corrected sum gate of all the transitions feeding the ground state was used to determine the intensities of the remaining transitions below the isomers. The intensities of the transitions below the isomers were normalized using the relative intensity of the 441-keV  $\gamma$  ray.

The relative intensities of the  $\gamma$ -ray transitions above the isomers were determined as follows. As discussed in the earlier sections, the 780-keV transition is a doublet; (i)  $25/2^- \rightarrow 21/2^-$  transition feeding the  $21/2^-$  level at 1495 keV, and (ii)  $33/2^+ \rightarrow 29/2^+$  transition which feeds directly to the  $29/2^+$  isomer at 2385 keV. The summed intensity of the 780-keV peak was obtained from single-fold data and normalized with respect to the relative intensity of the 643-keV transition. Further, an individual relative intensity of the bypassing 780-keV [ $25/2^- \rightarrow 21/2^-$ ] transition was deduced in a gate of the 262-keV  $\gamma$  ray. It may be noted that the second 780-keV transition, which populates the  $29/2^+$  isomer, was not observed in the prompt coincidence (100 ns) with the transitions following the decay of the  $29/2^+$  isomer (see Fig. 8). Thus, the intensity obtained with the gate on the 262-keV transition corresponds only to the relative intensity of the  $25/2^- \rightarrow 21/2^-$ , 780-keV transition. The relative intensity of the second 780-keV transition could then be determined by subtracting the contribution of the relative intensity of the bypassing 780-keV transition from the summed relative intensity. Further, the intensity of the 835-keV transition above the  $29/2^+$  isomer was determined from the ratio of the intensities of the 780-keV and 835-keV transitions in a *delayed* gate of the 488-keV  $\gamma$  ray [see Fig. 9(a)]. The intensity of the 784-keV  $\gamma$  ray, relative to the total  $\gamma$ -ray intensity

of the 643-keV transition, was also determined from the single-fold data. In order to deduce the relative intensity of the 389-keV  $\gamma$ -ray, the 389- and 784-keV peaks were fitted in a prompt coincidence spectrum with a gate on the 220-keV  $\gamma$  ray. The deduced intensities of both the transitions were normalized with respect to the relative intensity of the 784-keV transition which was obtained from single fold-data as discussed above. The relative intensities of the remaining transitions in the sequences “A”, “B”, “D”, and “E” were determined in efficiency corrected summed gates of the 780-, 784-, and 835-keV transitions and normalized with respect to the relative intensity of the 389-keV  $\gamma$  ray. The relative intensity of the 364-keV [ $37/2^{(-)} \rightarrow 35/2^-$ ] transition in sequence “B” is corrected for the branch which de-excites the 4252-keV level in sequence “C”. Moreover, the intensity of the second 364-keV  $\gamma$  ray, which populates the 3505-keV level was determined by subtracting the contribution of the upper 364-keV [ $37/2^{(-)} \rightarrow 35/2^-$ ] transition from the total relative intensity of the 364-keV doublet. The total relative intensity of the doublet was determined in a efficiency corrected summed prompt spectrum obtained with gates on the 780-, 784-, 835-, 1192-, and 569-keV transitions.

Finally, the relative intensities of the 1192-, 569-, 623-, 181-, 380-, and 197-keV transitions of sequence “C” were also deduced by fitting these transitions in a gate of the 220-keV  $\gamma$  ray. The relative intensity of the 784-keV transition (obtained from single-fold data) was used for normalization to deduce the relative intensities of the above transitions.

## IV. DISCUSSION

Nuclear structure investigations in the region around the doubly closed-shell nucleus  $^{208}\text{Pb}$  are of immense interest as a variety of nuclear structure aspects have been observed in this region. In particular, the level structure in At isotopes with a few neutron-holes with respect to the  $N = 126$  shell closure is governed by single-particle excitations [17–21]. Furthermore, shears bands have been reported in the lighter At isotopes viz.,  $^{201,203,204}\text{At}$  [12, 13, 44]. A similar sequence of  $\Delta I = 1$  transitions had also been reported in  $^{205}\text{At}$  [15]. However, the shears structure of the observed sequence was not confirmed [15]. On the other hand, the lighter Po and At nuclei are known to exhibit oblate and prolate deformed shapes [4, 10]. Thus, a systematic study across the isotopic chain enhances the understanding of shape evolution with decreasing neutron number. In  $^{207}\text{At}$ , which is the subject of the present work, the excited states only up to the  $25/2^+$  isomer at 2117 keV were known [16]. The present study reports an extended level scheme of  $^{207}\text{At}$ . In addition to several new transitions below the isomer, four new sequences are identified which feed the known  $25/2^+$  isomer. Moreover, the new  $29/2^+$  isomer is also established at 2385 keV, which completes the systematics

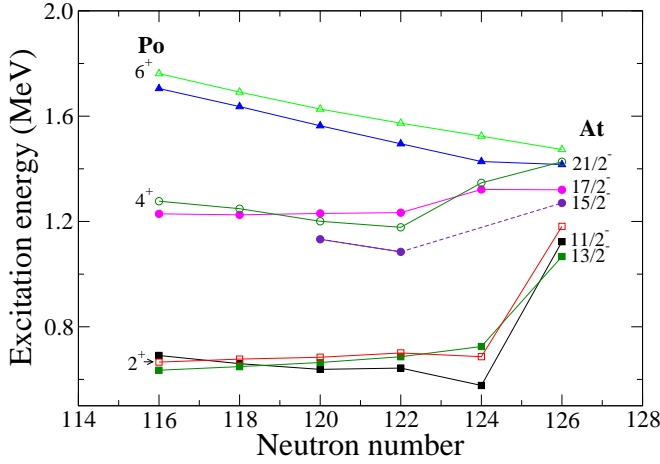


FIG. 10. Energy systematics of selected low-lying states in At (solid symbols) and Po (open symbols) isotopes. The excitation energies of the states in At and Po isotopes are taken from present work and Refs. [12–14, 20, 21, 28, 30, 42, 43].

of this isomer in odd- $A$  At isotopes. The proposed level scheme is understood in the framework of the shell-model approach. The yrast and near-yrast states in  $^{207}\text{At}$  are also compared with the systematics of the corresponding states in Po and odd- $A$  At isotopes for a qualitative understanding as discussed in the following sections.

Large-scale shell model calculations have been performed with the KHM3Y effective interaction [45], which was developed for the  $Z = 50$ – $126$ ,  $N = 82$ – $184$  model space. The model space comprised of 24 orbitals in total; the proton orbitals include  $g_{7/2}$ ,  $d_{5/2}$ ,  $h_{11/2}$ ,  $d_{3/2}$ ,  $s_{1/2}$  below the  $Z = 82$  and  $h_{9/2}$ ,  $f_{7/2}$ ,  $i_{13/2}$ ,  $f_{5/2}$ ,  $p_{3/2}$ ,  $p_{1/2}$  above it, while the neutron orbitals involve  $i_{13/2}$ ,  $p_{3/2}$ ,  $f_{5/2}$ ,  $p_{1/2}$ ,  $h_{9/2}$ ,  $f_{7/2}$  below the  $N = 126$  and  $g_{9/2}$ ,  $i_{11/2}$ ,  $j_{15/2}$ ,  $g_{7/2}$ ,  $d_{5/2}$ ,  $d_{3/2}$ ,  $s_{1/2}$  above. The cross-shell two-body matrix elements (TBMEs) are based on the M3Y interaction [46]. The neutron-proton particle-particle and hole-hole TBMEs use the Kuo-Herling interaction [47] as modified in Ref. [48]. In order to make the calculation feasible, the proton orbitals below the  $Z = 82$  shell closure were completely filled and the neutron excitations across the  $N = 126$  shell were not allowed. The calculations were performed using the shell model code NuShellX [49]. Recently, the experimental results of  $^{207}\text{Tl}$  [50–52] and  $^{208}\text{Pb}$  [45, 52] were interpreted using the shell model calculations which also used the same interaction mentioned above.

### A. States below the isomers

Figure 10 depicts the energy systematics of the yrast negative-parity states, viz.  $11/2^-$ ,  $13/2^-$ ,  $15/2^-$ ,  $17/2^-$ , and  $21/2^-$ , in odd- $A$  At isotopes, which is compared with the  $2^+$ ,  $4^+$ , and  $6^+$  states of the corresponding Po isotones. It is evident from the figure that the  $(11/2^-$ ,

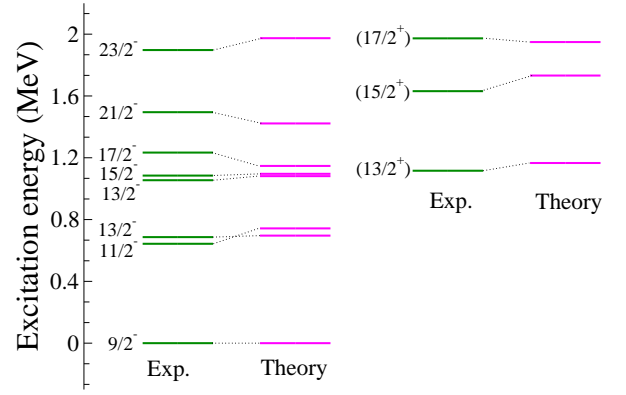


FIG. 11. Comparison of the experimental level energies of the yrast and near-yrast states below the isomers with those predicted from the shell model calculations.

$13/2^-$ ),  $(15/2^-$ ,  $17/2^-)$ , and  $21/2^-$  states in odd- $A$  At isotopes closely follow the trend in excitation energies of the  $2^+$ ,  $4^+$ , and  $6^+$  states in the corresponding Po isotones, respectively. The observed similarity in the excitation energies of the yrast states suggests that the low-lying negative parity states in odd- $A$  At isotopes can be understood in terms of the coupling of an unpaired proton in  $h_{9/2}$  orbital to the respective states of the even-even Po core. A similar interpretation is noted to explain the low-lying negative-parity states in neighboring odd- $A$  At isotopes [11–15]. Also, a sudden increase in the excitation energy of the  $11/2^-$  and  $13/2^-$  [ $2^+(^{210}\text{Po}) \otimes \pi h_{9/2}$ ] states may be noted, as opposed to the same states in the lighter isotopes where excitation energies are found to be rather constant. The marked difference in the excitation energies of the yrast states in the  $N = 126$  isotones relative to those in the lighter isotopes can be attributed to the difference in their configurations. The low-lying yrast states in the closed neutron shell nuclei, viz.  $^{210}\text{Po}$  and  $^{211}\text{At}$  are governed by pure proton configurations, while both proton-particle and neutron-hole excitations are expected to play a role in the lighter Po and At isotopes. The yrast states in  $^{211}\text{At}$  ( $N = 126$ ) are well understood in terms of the  $\pi(h_{9/2}^3)$ ,  $\pi(h_{9/2}^2 f_{7/2})$ , and  $\pi(h_{9/2}^2 i_{13/2})$  configurations [21].

Figure 11 shows a comparison of the experimental level energies of the yrast and near-yrast states below the isomers with those predicted from the shell-model calculations. It is evident from the figure that the experimental level energies are in good agreement (within 100 keV) with the shell-model predictions. The low-lying negative parity states viz.  $11/2^-$ ,  $13/2^-$ ,  $15/2^-$ ,  $17/2^-$ , and  $21/2^-$  are predicted to originate from the  $\pi(h_{9/2}^3) \otimes \nu(f_{5/2}^{-2} p_{1/2}^{-2})$  configuration. The energy systematics of these states in Po and At isotopes also suggests the same configuration as discussed above. The primary configuration (with 25.6% parentage) for the  $23/2^-$  state is predicted to be  $\pi(h_{9/2}^2 f_{7/2}) \otimes \nu(f_{5/2}^{-2} p_{1/2}^{-2})$ . It may be

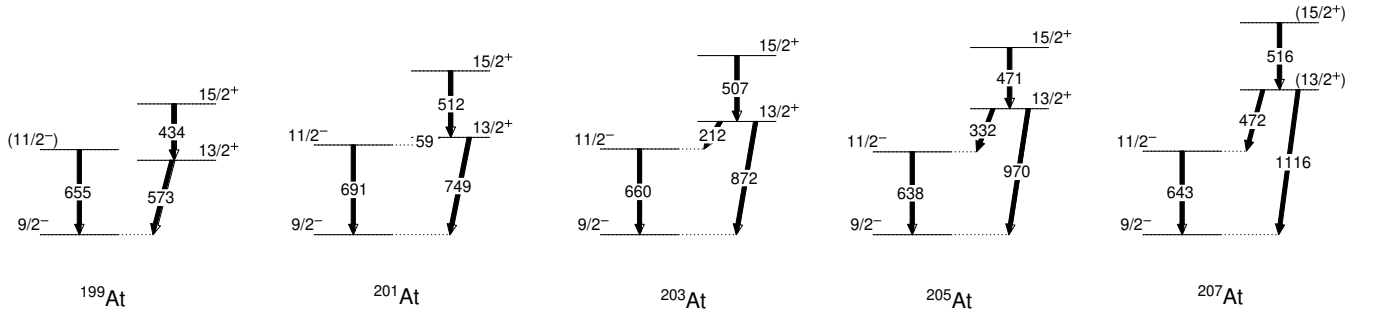


FIG. 12. Evolution of the  $13/2^+$  state in odd- $A$  At isotopes with increasing neutron number between  $114 \leq N \leq 122$ . The experimental information of the presented levels of the  $^{199-207}\text{At}$  nuclei are taken from the present work and Refs. [12–16, 22].

noted that only the states with firm spin-parity assignments are compared with the shell model calculations, except the  $(13/2^+)$ ,  $(15/2^+)$ , and  $(17/2^+)$  states. The positive parity of these states is suggested from the similarity in the level structures in odd- $A$  At isotopes as discussed below.

The  $13/2^+$  state, which originates from the  $\pi(i_{13/2})$  configuration, has been identified in several odd- $A$  At isotopes [10–15, 21, 22]. Figure 12 illustrates the evolution of the  $13/2^+$  state with increasing neutron number in At isotopes with  $114 \leq N \leq 122$ . It is observed that the excitation energy of the  $13/2^+$  state increases with increasing number of neutrons. However, the excitation energy of the  $11/2^-$  state remains nearly constant as shown in Fig. 12. A similar trend in the excitation energy of the  $13/2^+$  state has also been reported in odd- $A$  Bi isotopes [53–55]. This feature is explained by the coupling of the unpaired proton in the  $i_{13/2}$  orbital to the increasing number of valence neutron holes. The interaction of the  $\pi\nu^{-1}$  configuration for both the particles and holes in the  $i_{13/2}$  orbital has the smallest repulsion, which brings the  $13/2^+$  state down in energy with a decreasing number of neutrons [11, 56]. In  $^{199}\text{At}$ , the  $13/2^+$  state deexcites to the ground state only via an  $M2$  branch unlike the heavier isotopes, viz.  $^{201,203,205}\text{At}$ , where it is observed to decay via  $E1$  and  $M2$  transitions to the  $11/2^-$  and  $9/2^-$  ground state, respectively. A similar structure is also observed in  $^{207}\text{At}$ , where the 1116-keV state de-excites via the 472- and 1116-keV  $\gamma$  rays to the  $11/2^-$  level at 643 keV and the ground state, respectively. The observed similarities in the excitation energy and the decay paths of the 1116- and 1631-keV levels in  $^{207}\text{At}$  with the kindred states in the neighboring At isotopes suggest that these states are also likely to have positive parity. As illustrated in Fig. 11, the excitation energies of the proposed positive parity states viz.  $(13/2^+)$ ,  $(15/2^+)$ , and  $(17/2^+)$ , are in very good agreement with the shell model calculations, which suggest a dominant  $\pi(h_{9/2}^2 i_{13/2}) \otimes \nu(f_{5/2}^{-2} p_{1/2}^{-2})$  configuration for the states under consideration.

### B. Isomers and their decay properties

The region around the doubly-magic nucleus  $^{208}\text{Pb}$  is rich in nuclear isomerism [23]. The presence of high- $j$  valence orbitals leads to the realization of isomeric states in this region which arise due to dominant intrinsic degrees of freedom. An isomer ( $38^+$ ) in  $^{212}\text{Rn}$  ( $N = 126$ ) at  $E_x = 12.5$  MeV is the highest-lying isomer known to date [57]. This isomer results from the triple-core excitations coupled with the aligned valence protons. Several high-spin isomeric states have been reported in Po, At, and Fr isotopes [23]. A  $25/2^+$  isomer is reported in  $^{203,205,207}\text{At}$  isotopes [13–16]. Also, a long-lived  $29/2^+$  state is known in all odd- $A$  At isotopes with  $114 \leq N \leq 126$ , except in  $^{207}\text{At}$  [12–21]. As discussed in the Sec. III, we have identified the long-lived  $29/2^+$  isomeric state in  $^{207}\text{At}$  at  $E_x = 2385$  keV.

The high-spin isomers in odd- $A$  At isotopes may be interpreted in terms of the coupling of an unpaired proton in specific orbitals to the even-even core of the corresponding Po isotones. The  $11^-$  and  $9^-$  isomeric states have been reported in even-even Po isotopes, which originate from the  $\pi(h_{9/2}^1 i_{13/2}^1)_{11^-}$  two-quasi-proton and  $\nu(f_{5/2}^{-1} i_{13/2}^{-1})_{9^-}$  two-neutron-hole configurations, respectively [24, 42, 43, 58]. Figure 13(a) illustrates the energy systematics of the  $11^-$ ,  $9^-$ , and the subsequent  $8^+$  states in the even-even Po isotopes, which is compared with the corresponding  $29/2^+$ ,  $25/2^+$ , and  $23/2^-$  levels in the odd- $A$  At isotones. The systematic trend in the excitation energies suggests that the structure of the  $29/2^+$  and  $25/2^+$  isomeric states in  $^{207}\text{At}$  may be interpreted in terms of a weak coupling of an unpaired proton in the  $h_{9/2}$  orbital to the  $11^-$  and  $9^-$  isomers in  $^{206}\text{Po}$ , respectively. Similarly, the  $23/2^-$  state may be realized from a weak coupling of the unpaired proton in the  $f_{7/2}$  orbital to the  $8^+$  state of the Po core. Similar considerations have been used to explain the origin of the isomeric states in other odd- $A$  At isotopes [11–15, 17–22].

The  $25/2^+$  isomer in  $^{207}\text{At}$  de-excites to the  $23/2^-$  state via the 220-keV  $E1$  transition. The experimental  $B(E1)$  value for the 220-keV transition is  $3.6(9) \times 10^{-7} e^2 fm^2$ , which is hindered by seven orders of magnitude



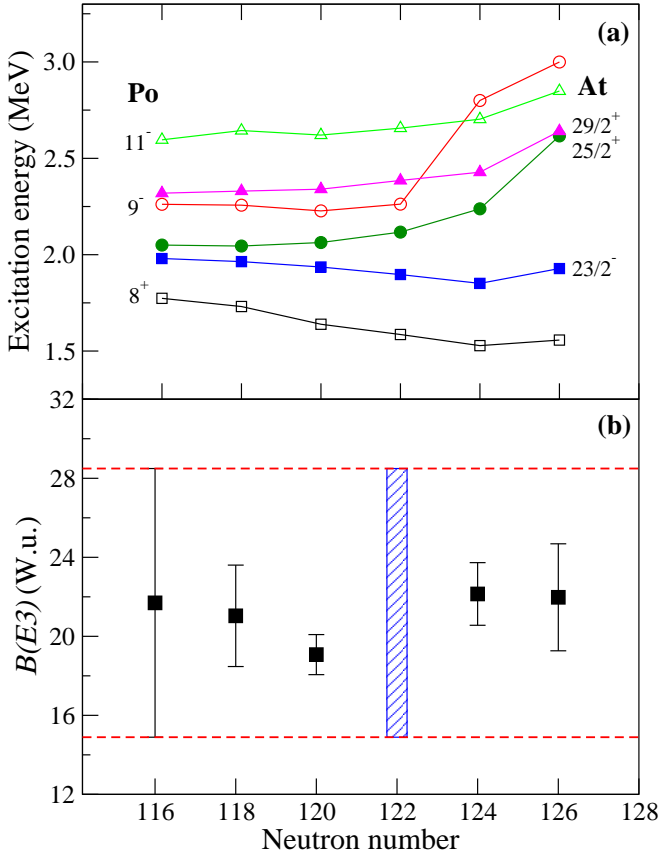


FIG. 13. (a) Energy systematics of the  $29/2^+$ ,  $25/2^+$  isomers and the  $23/2^-$  state in odd- $A$  At isotopes (solid symbols) and the  $11^-$ ,  $9^-$  and  $8^+$  states of the corresponding Po (open symbols) isotones. Panel (b) of the figure presents the variation of the experimental  $B(E3)$  values for the  $29/2^+ \rightarrow 23/2^-$  transition in odd- $A$  At isotopes with increasing neutron number. The shaded area indicates the possible range of the  $B(E3)$  value for the 488-keV transition in  $^{207}\text{At}$ . The experimental information for the At and Po isotopes is taken from the present work and Refs. [28, 30, 42, 43, 59–63].

with respect to the single-particle estimate. The hindrance in the decay of the  $25/2^+$  state may be attributed to a considerable difference in the wave functions of the  $25/2^+$  and  $23/2^-$  states. In  $^{203,205}\text{At}$ , the  $25/2^+$  isomer de-excites via competing  $E1$  and  $E2$  transitions unlike the one in  $^{207}\text{At}$  where only an  $E1$  decay branch is observed [13–15].

The systematics of the excitation energy and the decay path for the newly identified  $29/2^+$  isomer is observed to account well for its proposed spin-parity when compared to the same state in the neighboring odd- $A$  At isotopes. In the lighter At isotopes, viz.  $^{201,203,205}\text{At}$ , the  $29/2^+$  isomer is known to de-excite via  $E2$  and  $E3$  transitions to the subsequent  $25/2^+$  and  $23/2^-$  levels, respectively [12–15], while it decays only via an  $E2$  branch in  $^{199}\text{At}$  [11]. It has been observed that the  $E2$  decay-branch becomes weaker with increasing neutron number. The  $29/2^+$  iso-

mer in  $^{209}\text{At}$  is known to decay only via an  $E3$  transition [17–20]. However, in the case of  $^{211}\text{At}$  this isomer is reported to deexcite via an unobserved low-energy  $E2$  transition, in addition to a strong  $E3$  decay path [21, 64]. The proposed  $29/2^+$  isomeric level in  $^{207}\text{At}$  is also observed to decay via the 488-keV  $E3$  transition. However, the present data do not provide any conclusive evidence for an  $E2$  decay branch.

As mentioned earlier, the direct measurement of the half-life of the  $29/2^+$  isomer was not possible. However, the systematics of the  $E3$  transition strengths in odd- $A$  At isotopes can be used to determine the range of the expected half-life. Figure 13(b) depicts the variation of the  $B(E3)$  values corresponding to the  $29/2^+ \rightarrow 23/2^-$  transitions in odd- $A$  At isotopes with increasing neutron number. It may be noticed that the plotted  $B(E3)$  values are roughly constant. The observed striking similarities in the properties of the  $29/2^+$  isomer in odd- $A$  At isotopes as discussed above suggest that the transition strength of the 488-keV ( $29/2^+ \rightarrow 23/2^-$ )  $E3$  transition in  $^{207}\text{At}$  can assume a value between the range displayed by the shaded area in Fig. 13(b). This range of  $B(E3)$  values in turn suggests a half-life between 2–4  $\mu\text{s}$  for the  $29/2^+$  isomer in  $^{207}\text{At}$ . It is worth mentioning that the rough estimate of the half-life ( $\approx 3.5 \mu\text{s}$ ) for the  $29/2^+$  state as outlined in the previous section is consistent with the above range.

The shell-model calculations suggest that the  $29/2^+$  and  $23/2^-$  levels are three quasi-proton states with  $\pi(h_{9/2}^2 i_{13/2}^1)$  and  $\pi(h_{9/2}^2 f_{7/2}^1)$  primary configurations, respectively. The  $25/2^+$  isomer is associated with the  $\pi(h_{9/2}^3)_{9/2^-} \otimes \nu(f_{5/2}^{-1} i_{13/2}^{-1})_{9^-}$  configuration and originates from a weak coupling of the  $\pi h_{9/2}$  with two-quasi-neutron-hole configuration. Further, it was observed that the shell-model calculations account well for excitation energies of the  $23/2^-$  and  $25/2^+$  states, while an underestimation by 295 keV is observed for the  $29/2^+$  isomer. It may be noted that the  $29/2^+$  isomer decays via the 488-keV  $E3$  transition, which corresponds to the  $\pi(i_{13/2} \rightarrow f_{7/2})$  transition as suggested by the shell-model configurations for the states under consideration. In such cases, where the initial and final state wave-functions involve the high- $j$  proton ( $i_{13/2}$  and  $f_{7/2}$ ) and neutron ( $j_{15/2}$  and  $g_{9/2}$ ) orbitals which differ by  $\Delta j = \Delta l = 3$ , the configuration of initial state is likely to have a mixing of the  $3^-$  octupole phonon of the  $^{208}\text{Pb}$  coupled with the final state [65]. Therefore, the corresponding  $E3$  transitions are expected to be very fast [65]. Such states have been observed in a number of nuclei around the doubly-closed  $^{208}\text{Pb}$  [50, 52, 66]. The  $29/2^+$  isomeric level in  $^{207}\text{At}$  also appears to have a mixing of the octupole vibrational phonon. A recent study by Berry *et al.* reported that the states involving octupole vibrations in the region around  $^{208}\text{Pb}$  are underestimated ( $\approx 250$  keV) by the shell-model calculations performed using the KHM3Y effective interaction [50]. A similar effect is also observed in the calculations for the  $29/2^+$  state in  $^{207}\text{At}$ .



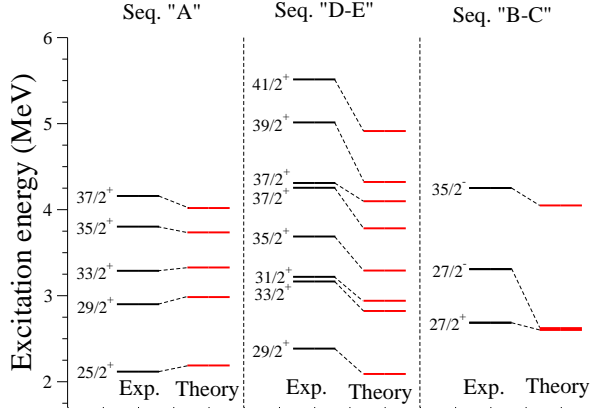


FIG. 14. Comparison of the experimental level energies of yrast and near-yrast states above the isomers with that predicted by the shell-model calculations. Only those states for which firm spin-parities are known are considered for the comparison.

### C. States above the isomers

Figure 14 shows a comparison of the excitation energies of the yrast and near-yrast states above the  $25/2^+$  isomer with the shell-model calculations. The shell-model states corresponding to the experimental levels in a specific sequence are chosen on the basis of configurations. As discussed in the previous section, the isomeric  $25/2^+$  state is associated with the  $\pi(h_{9/2}^3)_{9/2^-} \otimes \nu(f_{5/2}^{-1}i_{13/2}^{-1})_9$  configuration. The same configuration is observed to account well (within 150 keV), as shown in Fig. 14, for the higher-lying states in sequence “A” by breaking of the proton pair in the  $h_{9/2}$  orbital. A similar sequence has also been reported in  $^{205}\text{At}$ , which feeds the  $25/2^+$  isomer at 2063 keV [15]. However, no such sequence was observed in  $^{203}\text{At}$  [13].

As mentioned earlier, the  $29/2^+$  isomeric level is predominantly the three quasi-proton state with a maximum possible angular momentum from the  $\pi(h_{9/2}^2i_{13/2})$  configuration. For the realization of the states above the  $29/2^+$  isomer, the neutron-hole pairs may contribute in the angular-momentum generation. Therefore, the shell-model states originating from the  $\pi(h_{9/2}^2i_{13/2})_{29/2^+} \otimes I_n$  configuration, where  $I_n$  is the contribution to the angular momentum from the neutron holes are compared with the states in sequences “D” and “E”. As shown in Fig. 14, a systematic underestimation is observed in the calculated excitation energies of the states in sequences “D” and “E”. It was further noticed that the deviation between the experiment and the shell-model calculations increases with excitation energy, which may be attributed to the truncation scheme adopted for the calculations, due to computational limitations. The states in sequences “B”

and “C” are found to be in rather good agreement with the shell-model calculations, except the  $27/2^-$  state.

Moreover, the available spectroscopic information on the states above the  $29/2^+$  isomer is scarce in the neighboring odd- $A$  At isotopes for a systematic comparison.

## V. SUMMARY

Excited states above the known  $25/2^+$  isomer in  $^{207}\text{At}$  have been investigated for the first time using the  $^{198}\text{Pt}(^{14}\text{N}, 5n\gamma)^{207}\text{At}$  reaction. The half-life of the  $25/2^+$  isomer is revisited and a value of  $T_{1/2} = 107.5(9)$  ns is inferred, which is consistent with that reported by Sjoreen *et al.* [16]. The level scheme is considerably extended up to 6.5 MeV and  $47/2\hbar$  with the addition of about 60 new  $\gamma$ -ray transitions. A long-lived  $29/2^+$  isomeric state ( $E_x = 2385$  keV) is established for the first time in  $^{207}\text{At}$ , with a similar level having been identified earlier in the neighboring odd- $A$  At isotopes. The half-life of the proposed  $29/2^+$  isomer is estimated to be in the 2–4  $\mu\text{s}$  range on the basis of the systematics of the  $B(E3)$  values corresponding to the  $E3$  transitions, which de-excite the  $29/2^+$  isomer in the neighboring odd- $A$  At isotopes. Furthermore, the 1116-keV level is suggested to originate from the  $\pi(i_{13/2})$  configuration on the basis of similarities in its excitation energy and decay paths with that of the  $13/2^+$  state in the neighboring odd- $A$  At isotopes. The large-scale shell-model calculations were performed using the shell-model code NuShellX with the KHM3Y effective interaction. An overall good agreement has been observed between the experimental results and the shell-model predictions for the states below the isomers and those in sequence “A” above the  $25/2^+$  isomer. However, the shell-model calculations appear to significantly underestimate the excitation energies of the remaining states. In addition, the weak coupling of an unpaired proton in the  $h_{9/2}$  or  $f_{7/2}$  orbitals with the states of  $^{206}\text{Po}$  core is observed to qualitatively account for the level structure in  $^{207}\text{At}$ . An experiment to determine half-life of the  $29/2^+$  isomer is in order.

## VI. ACKNOWLEDGMENTS

The authors would like to thank the technical staff from IUAC for their support during the experiment. The financial support by DST, India (Grant No. IR/S2/PF-03/2003-III) for the INGA project is also acknowledged. K. Y. acknowledges the financial assistance from MHRD, India. A. Y. D. and D. S. would like to acknowledge the financial support by SERB (DST), Grant No. CRG/2020/002169. Madhu acknowledges financial support from DST, India under the INSPIRE fellowship scheme (IF 180082). P.C.S. acknowledges a research grant from SERB (India), CRG/2019/000556.

- 
- [1] K. Heyde, P. Van Isacker, M. Waroquier, J. L. Wood, and R. A. Meyer, *Phys. Rep.* **102**, 291 (1983).
- [2] J. L. Wood, K. Heyde, W. Nazarewicz, M. Huyse, and P. Van Duppen, *Phys. Rep.* **215**, 101 (1992).
- [3] R. Julin, K. Helariutta, and M. Muikku, *J. Phys. G: Nucl. Part. Phys.* **27**, R109 (2001).
- [4] K. Helariutta et al., *Eur. Phys. J. A* **6**, 289 (1999).
- [5] M. J. A. de Voigt, J. Dudek, and Z. Szymanski, *Rev. Mod. Phys.* **55**, 949 (1983).
- [6] T. Grahn, J. Pakarinen, L. Jokiniemi, M. Albers, K. Auranen, C. Bauer, C. Bernards, A. Blazhev, P. A. Butler, S. Bönig, A. Damyanova, T. De Coster, H. De Witte, J. Elseviers, L. P. Gaffney, M. Huyse, A. Herzán, U. Jakobsson, R. Julin, N. Kesteloot et al., *Eur. Phys. J. A* **52**, 340 (2016).
- [7] M. Stoyanova, G. Rainovski, J. Jolie, N. Pietralla, A. Blazhev, M. Beckers, A. Dewald, M. Djongolov, A. Es-maylzadeh, C. Fransen, L. M. Gerhard, K. A. Gladnishki, S. Herb, P. R. John, V. Karayonchev, J. M. Keatings, R. Kern, L. Knafla, D. Kocheva, L. Kornwebel, Th. Kroll, M. Ley, K.M.Mashtakov, C.Muller-Gatermann, J. -M. Regis, M. Scheck, K. Schomacker, J. Sinclair, P. Spagnoletti, C. Surder, N. Warr, V. Werner, and J. Wiederhold, *Phys. Rev. C* **100**, 064304 (2019).
- [8] K. Van de Vel, A. Andreyev, R. Page, H. Kettunen, P. T. Greenlees, P. Jones, R. Julin, S. Juutinen, H. Kankaanpää, A. Keenan, P. Kuusiniemi, M. Leino, M. Muikku, P. Nieminen, P. Rahkila, J. Uusitalo, K. Eskola, A. Hürstel, M. Huyse, Y. L. Coz, M. Smith, P. V. Duppen, and R. Wyss, *Eur. Phys. J. A* **17**, 167 (2003).
- [9] M. Nyman, S. Juutinen, I. Darby, S. Eeckhaudt, T. Grahn, P. T. Greenlees, U. Jakobsson, P. Jones, R. Julin, S. Ketelhut, H. Kettunen, M. Leino, P. Nieminen, P. Peura, P. Rahkila, J. Sarén, C. Scholey, J. Sorri, J. Uusitalo, and T. Enqvist, *Phys. Rev. C* **88**, 054320 (2013).
- [10] K. Andgren, U. Jakobsson, B. Cederwall, J. Uusitalo, T. Bäck, S. J. Freeman, P. T. Greenlees, B. Hadinia, A. Hugues, A. Johnson, P. M. Jones, D. T. Joss, S. Juutinen, R. Julin, S. Ketelhut, A. Khaplanov, M. Leino, M. Nyman, R. D. Page, P. Rahkila, M. Sandzelius, P. Sapple, J. Sarén, C. Scholey, J. Simpson, J. Sorri, J. Thomson, and R. Wyss, *Phys. Rev. C* **78**, 044328 (2008).
- [11] U. Jakobsson, J. Uusitalo, S. Juutinen, M. Leino, P. Nieminen, K. Andgren, B. Cederwall, P. T. Greenlees, B. Hadinia, P. Jones, R. Julin, S. Ketelhut, A. Khaplanov, M. Nyman, P. Peura, P. Rahkila, P. Ruotsalainen, M. Sandzelius, J. Sarén, C. Scholey, and J. Sorri, *Phys. Rev. C* **82**, 044302 (2010).
- [12] K. Auranen, J. Uusitalo, S. Juutinen, U. Jakobsson, T. Grahn, P. T. Greenlees, K. Hauschild, A. Herzan, R. Julin, J. Konki, M. Leino, J. Pakarinen, J. Partanen, P. Peura, P. Rahkila, P. Ruotsalainen, M. Sandzelius, J. Saren, C. Scholey, J. Sorri, and S. Stolze, *Phys. Rev. C* **91**, 024324 (2015).
- [13] K. Auranen, J. Uusitalo, S. Juutinen, H. Badran, F. Defranchi Bisso, D. Cox, T. Grahn, P. T. Greenlees, A. Herzan, U. Jakobsson, R. Julin, J. Konki, M. Leino, A. Lightfoot, M. J. Mallaburn, O. Neuvonen, J. Pakarinen, P. Papadakis, J. Partanen, P. Rahkila, M. Sandzelius, J. Saren, C. Scholey, J. Sorri, S. Stolze, and Y. K. Wang, *Phys. Rev. C* **97**, 024301 (2018).
- [14] T. P. Sjoreen, D. B. Fossan, U. Garg, A. Neskakis, A. R. Poletti, and E. K. Warburton, *Phys. Rev. C* **25**, 889 (1982).
- [15] R. F. Davie, A. R. Poletti, G. D. Dracoulis, A. P. Byrne, and C. Fahlander, *Nucl. Phys. A* **430**, 454 (1984).
- [16] T. P. Sjoreen, U. Garg, and D. B. Fossan, *Phys. Rev. C* **23**, 272 (1981).
- [17] T. P. Sjoreen, G. Schatz, S. K. Bhattacharjee, B. A. Brown, D. B. Fossan, and P. M. S. Lesser, *Phys. Rev. C* **14**, 1023 (1976).
- [18] J. Adam, A. Kuklik, A. Spalek, D. Venos, and M. J. Kuznetsova, *Czech. J. Phys. B* **28**, 857 (1978).
- [19] V. Rahkonen and T. Lonnroth, *Z. Phys. A* **322**, 333 (1985).
- [20] P. Mukherjee, P. Sen, I. Mukherjee, and C. Samanta, *J. Phys. G* **16**, L107 (1990).
- [21] S. Bayer, A. P. Byrne, G. D. Dracoulis, A. M. Baxter, T. Kibédi, and F. G. Kondev, *Nucl. Phys. A* **694**, 3 (2001).
- [22] K. Dybdal, T. Chapuran, D. B. Fossan, W. F. Piel, D. Horn, and E. K. Warburton, *Phys. Rev. C* **28**, 1171 (1983).
- [23] A. K. Jain, B. Maheshwari, S. Garg, M. Patial, and B. Singh, *Nucl. Data Sheets* **128**, 1 (2015).
- [24] H. Beuscher, D. R. Zolnowski, D. R. Haenni, and T. T. Sugihara, *Phys. Rev. Lett.* **36**, 19 (1976).
- [25] A. M. Baxter, A. P. Byrne, G. D. Dracoulis, R. A. Bark, F. Riess, A. E. Stuchbery, M. C. Kruse, and A. R. Poletti, *Nucl. Phys. A* **515**, 3 (1990).
- [26] V. Rahkonen, B. Fant, C. J. Herrlander, *Phys. Scr.* **34**, 720 (1986).
- [27] B. Fant, T. Weckstrom, and A. Kallberg, *Phys. Scr.* **41**, 652 (1990).
- [28] V. Rahkonen and T. Lönnroth, *Nucl. Phys. A* **464**, 3 (1987).
- [29] R. G. Helmer and C. W. Reich, *Phys. Rev. C* **27**, 2248 (1983).
- [30] N. Bijnens, P. Decrock, S. Franchoo, M. Gaelens, M. Huyse, H.-Y. Hwang, I. Reusen, J. Szerypo, J. von Schwarzenberg, G. Vancraeynest, P. Van Duppen, and J. Wauters, *Phys. Rev. C* **58**, 754 (1998).
- [31] O. Häusser, T. K. Alexander, J. R. Beene, E. D. Earle, A. B. McDonald, F. C. Khanna, and I. S. Towner, *Nucl. Phys. A* **273**, 1 (1976).
- [32] S. Nagamiya and T. Inamura, *Nucl. Phys. A* **182**, 1 (1972).
- [33] S. Muralithar *et al.*, *Nucl. Instr. and Meth. A* **622**, 12 (2000).
- [34] Mamta Jain, E. T. Subramaniam, and Shouri Chatterjee, *Rev. Sci. Instrum.* **94**, 013304 (2023).
- [35] Rene Brun and Fons Rademakers, *Nucl. Inst. & Meth. in Phys. Res. A* **389**, 81-86 (1997).
- [36] D. C. Radford, *Nucl. Instrum. Methods Phys. Res., Sect. A* **361**, 297 (1995).
- [37] A. Krämer-Flecken, T. Morek, R. M. Lieder, W. Gast, G. Hebinghaus, H. M. Jäger, and W. Urban, *Nucl. Instrum. Methods Phys. Res., Sect. A* **275**, 333 (1989).
- [38] Khamosh Yadav, A. Y. Deo, Madhu, Pragati, P. C. Srivastava, S. K. Tandel, S. G. Wahid, S. Kumar, S. Muralithar, R. P. Singh, Indu Bala, S. S. Bhattacharjee, Ritika Garg, S. Chakraborty, S. Rai, and A. K. Jain, *Phys. Rev. C* **105**, 034307 (2022).

- [39] Pragati, A. Y. Deo, S. K. Tandel, S. S. Bhattacharjee, S. Chakraborty, S. Rai, S. G. Wahid, S. Kumar, S. Murallithar, R. P. Singh, Indu Bala, Ritika Garg, and A. K. Jain, *Phys. Rev. C* **97**, 044309 (2018).
- [40] G. Duchêne, F. A. Beck, P. J. Twin, G. de France, D. Curien, L. Han, C. W. Beausang, M. A. Bentley, P. J. Nolan, and J. Simpson, *Nucl. Instrum. Methods Phys. Res., Sect. A* **432**, 90 (1999).
- [41] J.-M. Régis, G. Pascovici, J. Jolie, and M. Rudigier, *Nucl. Instrum. Methods Phys. Res., Sect. A* **622**, 83 (2010).
- [42] A. R. Poletti, G. D. Dracoulis, A. E Byrne, A. E. Stuchbery, B. Fabricius, T. Kibédi, and EM. Davidson, *Nucl. Phys. A* **615** 95 (1997).
- [43] L. G. Mann, K. H. Maier, A. Aprahamian, J. A. Becker, D. J. Decman, E. A. Henry, R. A. Meyer, N. Roy, W. Stöfl, and G. L. Struble, *Phys. Rev. C* **38**, 74 (1988) and references therein.
- [44] D. J. Hartley, E. P. Seyfried, W. Reviol, D. G. Sarantites, C. J. Chiara, O. L. Pechenaya, K. Hauschild, A. Lopez-Martens, M. P. Carpenter, R. V. F. Janssens, D. Seweryniak, and S. Zhu, *Phys. Rev. C* **78**, 054319 (2008).
- [45] B. A. Brown, *Phys. Rev. Lett.*, **85**, 5300 (2000).
- [46] G. Bertsch, J. Borysowicz, H. McManus and W. G. Love, *Nucl. Phys. A* **284**, 399 (1977).
- [47] G. H. Herling and T. T. S. Kuo, *Nucl. Phys. A* **181**, 113 (1972).
- [48] E. K. Warburton and B. A. Brown, *Phys. Rev. C* **43**, 602 (1991).
- [49] B. A. Brown and W D M Rae, *Nucl. Data Sheets* **120**, 115 (2014).
- [50] T. A. Berry, Zs. Podolyák, R. J. Carroll, R. Lică, B. A. Brown, H. Grawe, Ch. Sotty, N. K. Timofeyuk, T. Alexander, A. N. Andreyev *et al.*, *Phys. Rev. C* **101**, 054311 (2020).
- [51] E. Wilson, Zs. Podolyák, H. Grawe, B. A. Brown, C. J. Chiara, S. Zhu, B. Fornal, R. V. F. Janssens, C. M. Shand, M. Bowry *et al.*, *Phys. Lett. B* **747**, 88 (2015).
- [52] Zs. Podolyák, C. M. Shand, E. Wilson, B. A. Brown, H. Grawe, C. J. Chiara, S. Zhu, B. Fornal, R. V. F. Janssens, M. Bowry *et al.*, *Journal of Physics: Conference Series* **580**, 012010 (2015).
- [53] T. Lönnroth, *Z. Phys. A* **307**, 175 (1982).
- [54] W. F. Piel, Jr., T. Chapuran, K. Dybdal, D. B. Fossan, T. Lonnroth, D. Horn, and E. K. Warburton, *Phys. Rev. C* **31**, 2087 (1985).
- [55] R. E. Stone, C. R. Bingham, L. L. Riedinger, R. W. Lide, H. K. Carter, R. L. Mlekodaj, and E. H. Spejewski, *Phys. Rev. C* **31**, 582 (1985).
- [56] T. Lönnroth, C. W. Beausang, D. B. Fossan, L. Hildingsson, W. F. Piel, Jr., M. A. Quader, S. Vajda, T. Chapuran, and E. K. Warburton, *Phys. Rev. C* **33**, 1641 (1986).
- [57] G. D. Dracoulis, G. J. Lane, A. P. Byrne, P. M. Davidson, T. Kibédi, P. H. Nieminen, H. Watanabe, A. N. Wilson, H. L. Liu, and F. R. Xu, *Phys. Rev. C* **80**, 054320 (2009).
- [58] A. Maj, H. Grawe, H. Kluge, A. Kuhnert, K. H. Maier, J. Recht, N. Roy, H. Hübel, and M. Guttormsen, *Nucl. Phys. A* **509**, 413 (1990).
- [59] F. G. Kondev, *Nucl. Data Sheets* **187**, 355 (2023).
- [60] F. G. Kondev, *Nucl. Data Sheets* **177**, 509 (2021).
- [61] F. G. Kondev, *Nucl. Data Sheets* **166**, 1 (2020).
- [62] J. Chen and F. G. Kondev, *Nucl. Data Sheets* **126**, 373 (2015).
- [63] B. Singh and D. Abriola and C. Baglin and V. Demetriou and T. Johnson and E. McCutchan and G. Mukherjee and S. Singh and A. Sonzogni and J. Tuli, *Nucl. Data Sheets* **114**, 661 (2014).
- [64] I. Bergström, B. Fant, C. J. Herrlander, K. Wikstrom, J. Blomqvist, *Phys. Scr.* **1**, 243 (1970).
- [65] I. Bergström and B. Fant, *Phys. Scr.* **31**, 26 (1985).
- [66] M. Rejmund, K. H. Maier, R. Broda, B. Fornal, M. Lach, J. Wrzesinski, J. Blomqvist, A. Gadea, J. Gerl, M. Gorska, H. Grawe, M. Kaspar, H. Schaffner, Ch. Schlegel, R. Schubart, H. J. Wollersheim, *Eur. Phys. J. A* **8**, 161 (2000).